aerospace

MDPI

Article

Conceptual Design and Optimization of Distributed Electric Propulsion General Aviation Aircraft

Jiang Wu [1,2], Feng Gao [1], Shengwen Li [3] and Fengtian Yang [1,2,*]

[1] Liaoning General Aviation Academy, Shenyang 110136, China; wujiangnuaa@163.com (J.W.)
[2] Shenyang Aircraft Design & Research Institute, Shenyang 110035, China
[3] AVIC Aerodynamics Research Institute, Shenyang 110034, China
* Correspondence: yang_ft_lgaa@163.com

Abstract: The interaction between the slipstream of the propellers and the wing of an aircraft with distributed electric propulsion (DEP) could benefit aerodynamics. A conceptual design and optimization are carried out in order to increase the range of an electric general aviation aircraft without affecting its takeoff and landing velocity in the same fuselage condition. Propellers are modelled using the actuator disk (AD) theory, and the aircraft is modelled using the vortex lattice method (VLM) to obtain DEP aircraft's aerodynamics in conceptual design. The DIRECT method is used for global optimization. To concentrate on the layout of the propellers and wing, a propeller with the same chord distribution, twist distribution, and number of blades is selected. The design and optimization of DEP aircraft's range is carried out with the objective of achieving the maximum product of the lift–drag ratio with propeller efficiency under force balance constrains. Additionally, to decrease the takeoff and landing distance, the DEP aircraft's takeoff and landing performance are optimized with the objective of the smallest velocity at an angle near the tail down angle under the constrains of acceleration bigger than 0 and a Mach number at the tip of blades smaller than 0.7. The CFD simulation was used to confirm the DEP aircraft's pretty accurate aerodynamics. Compared to the reference aircraft, the improved DEP aircraft with 10 high-lift propellers on the leading edge of the wing and 2 wing-tip propellers may boost cruise performance by 6% while maintaining takeoff and landing velocity. Furthermore, it has been shown that the stall speed of DEP aircraft with smaller wings would rise proportionally when compared to conventional design aircraft, and the power need of DEP aircraft will be increased as a result of the operation of high-lift propellers. The conceptual design and optimal approach suggested in this work has some reference value for the design and research of the fixed-wing DEP general aviation aircraft.

Keywords: distributed electric propulsion; conceptual design; optimization; range

Citation: Wu, J.; Gao, F.; Li, S.; Yang, F. Conceptual Design and Optimization of Distributed Electric Propulsion General Aviation Aircraft. *Aerospace* **2023**, *10*, 387. https://doi.org/10.3390/aerospace10050387

Academic Editor: Dimitri Mavris

Received: 21 February 2023
Revised: 3 April 2023
Accepted: 21 April 2023
Published: 22 April 2023

1. Introduction

Research and development for new energy electric aircrafts has become one of the most important fields in green aviation because of its environmentally friendly features, such as little noise and no emissions of greenhouse gases [1]. In the past ten years, a great deal of aircrafts that use electricity for either all or part of their propulsion have been built [2]. The specific energy of onboard energy storage systems, such as lithium-ion batteries, is a significant impediment to the development of all-electric aircrafts [3]. Distributed electric propulsion is currently viewed as the essential technology for electric aircrafts that become more powerful and achieve greater performance, despite limits in the specific energy of batteries and other issues [4]. It is even seen as a game changer in the field of electric aircraft construction due to improvements in aerodynamic efficiency, ruggedness, and payload [5].

The DEP aircraft, which is now the subject of extensive research, is a type of aircraft driven by several electric motors in conjunction with thrust-generating apparatuses, such as electrically powered fans or propellers [6]. TheX-57 is a well-known DEP aircraft

that NASA is currently researching and developing as a demonstration of the leading edge asynchronous propeller technology (LEAPTech) [7]. According to projections, the X-57 will use just 20% as much energy as the original aircraft [8]. The high aerodynamic performance of the DEP aircraft could be obtained through the interaction of aerodynamics and propulsion, and the efficiency of the propulsion system could be increased by the use of electric motors and battery systems in X-57 [9].

Before DEP was suggested, a few academics had investigated the interaction between the slipstream of the propellers and the wing. In [10], several results were reached on the role of factors in the interaction between the slipstream of propellers and the wing. To begin, the inboard up rotation of propellers at the tip of the wing was beneficial in increasing the lift–drag ratio. Second, a high position of the propellers' rotation axis to the top surface of the wing was excellent for a large lift coefficient, while a low location of the propellers' rotation axis to the upper surface of the wing was ideal for a high propeller efficiency. Thirdly, although a large distance was beneficial, the distance between the propellers and the leading edge of the wing had little bearing on the efficiency of the propellers. In a test conducted in [11], it was discovered that a layout with propellers moving inboard and up at the tip of the wing reduced the drag coefficient while increasing propeller thrust. For a CFD simulation with tractor propellers modeled as an actuator disk in [12], the average accuracy in the lift coefficient was 3.9% higher than the wind tunnel test, while the drag coefficient was practically the same. According to [13], the interaction between the slipstream of the tractor propeller and the wing might lower the drag of the wing by around 10%.

Several studies on the leading edge asynchronous propeller arrangement were carried out by NASA after the X-57's debut. At the LEAPTech ground tests conducted on the lakebed outside NASA's Armstrong Flight Research Mission Directorate in California in 2015, it was discovered that the lift coefficient of a wing may be more than doubly boosted with the action of high-lift propellers [14]. In the high-lift configuration, the performance of the X-57 was examined in FUN3D, USM3D, Kestrel, and STAR CCM+ [9], and it was discovered that the lift coefficient could be enhanced by about 170% and the generated drag coefficient could be lowered by about 7.5% [7]. The specifics for selecting high-lift propellers were investigated, and the mechanism for selecting the number of high-lift propellers in a system is presented in [15] for NASA's SCEPTOR DEP flying demonstrator. According to [16], high-lift propellers need to be properly built with a trade-off between the airfoil, blade planform parameters, and wing integration, such as a wing–nacelle offset for DEP aircrafts. In [17], a straightforward strategy for designing propellers that might improve wing lift considerably while producing little thrust and power was described. It was demonstrated that the propeller produced using this technique could use 15% less power and generate 11% less thrust than the one developed using the lowest induced loss method [17] for a NASA SCEPTOR flying demonstrator.

In addition to the X-57 research, a growing number of studies on the testing and simulation of DEP aircrafts' aerodynamics have also been conducted. In [18], a type of distributed electric-propelled propeller aircraft was presented, and the ways the distributed propeller slipstream effect affected the aerodynamic properties of the aircraft were discovered. A maximum increase in an aircraft's lift coefficient of more than 65% was demonstrated in [18]. A distributed propeller electric general aviation aircraft aerodynamic arrangement was demonstrated in [19], and slip grid technology was utilized to model the slipstream of the propellers. Additionally, in [19], the aerodynamic parameters of DEP aircrafts in the cruising state, takeoff state, and landing state were obtained based on the CFD simulation. In [20], a series of ground test platforms for the aerodynamic propulsion system of DEP aircrafts were constructed, and the performance of the power system, aerodynamic performance, and aerodynamic-propulsion coupling relationship of DEP technology were evaluated using ground test and numerical modeling. A rapid aerodynamic performance evaluation software was developed in [21] using the vortex grid methodology with viscosity correction and linear non-viscous aerodynamic coupling calculation methods. When compared to the CFD findings, the greatest error from the evaluation of the lift coefficient

and drag coefficient of single wing and single propeller/wing in [21] was less than 8.2%. In [22], an optimization approach for the distributed propeller layout design under the slipstream effects was given; a configuration with an optimized propeller layout had a lift coefficient gain of around 5.6% and a drag coefficient decrease of about 13.9%. In [23], optimization methods for conceptual and early design stages were reviewed, and the strategy for a propulsion number optimization was investigated to maximize overall efficiency in cruise. In [24], a low-cost aero-propulsive approach to study DEP aircrafts was created and utilized to assess the aero-propulsive effectiveness of DEP aircrafts in pusher and tractor propeller configurations. In [24], the wing was modeled using the vortex lattice technique, with the wake modeled using the VLM method with boundary corrections, and the propeller was modeled using the blade element method, with the slipstream represented using the vortex ring method. In [25], the aerodynamic performance of the DEP system was evaluated using wind tunnel experiments and computer simulations, and it was discovered that the stall of the DEP configuration could be delayed and the lift–drag ratio could drop before the stall when compared to an isolated wing. In [26], an aerodynamic analysis tool was created by adding a viscous correction to OpenVSP using a Python wrapper, and it was discovered that the lift and drag coefficients of the tool and those from the CFD solver were in excellent agreement. A low-order method to forecast the overall lift and lift distribution of a wing was presented in [27], and the method's outcomes were rather accurate when compared to those from the CFD simulation and testing before the stall. A multidisciplinary design optimization framework for a general aviation aircraft wing design that took into account the impact of a wing-mounted propeller was given in [28], and it demonstrated that superior designs could be obtained by taking this interaction into account. In [29], a strategy for improving the wing lift–drag ratio was developed by optimizing the propeller slipstream, and it was demonstrated that applying this method might enhance the wing lift–drag ratio at the expense of propeller efficiency. A program based on the vortex particle approach was created in [30–32] to study the interaction of the slipstream from several rotors. Based on the simulation outcomes of specific multirotor configurations, it was shown that the code might be used as a mid-fidelity modeling tool for the early design of distributed propulsion electric aircrafts.

As previously indicated, the possible benefits of the DEP design have been extensively researched. However, with the exception of the X-57, little research has been conducted on how to design a fixed-wing DEP aircraft that can profit from the interaction between the propeller's slipstream and the wing. In this study, a method for designing a fixed-wing DEP general aviation aircraft in the conceptual stage is proposed. The fixed-wing DEP aircraft under study here has a similar configuration to the X-57, which has tractor propellers installed on the leading edge of the wing and wingtip. The low-order analysis tool selected here is OpenVSP, in which the wings and aircraft are represented using the vortex lattice method and the propellers are treated as actuator disks. In Python, an optimization code is created using the DIRECT global optimization method. To precisely optimize the cruise performance of DEP aircrafts, the restrictions of force balancing are initially presented. In accordance with the method, the cruise, takeoff, and landing performance of DEP aircrafts is optimized. The design scheme of the DEP airplane is further examined in STAR CCM+ once concept design is complete. The performance of the aircraft is then determined accordingly to confirm the viability of the suggested strategy.

2. The Aerodynamic Interaction of the Wing and Tractor Propeller Slipstream

2.1. Effects of the Wing on the Propeller

Wings create an upstream effect by changing the inflow at the propeller disk owing to in-plane and out-of-plane generated velocities [33]. The in-plane velocities are primarily influenced by the wing's tail vortex system and bound vortex. The out-of-plane-induced velocity is a combination of the wing blockage and the velocity produced by the wing bound vortex [33]. Figure 1 depicts how the propeller and wing interact.

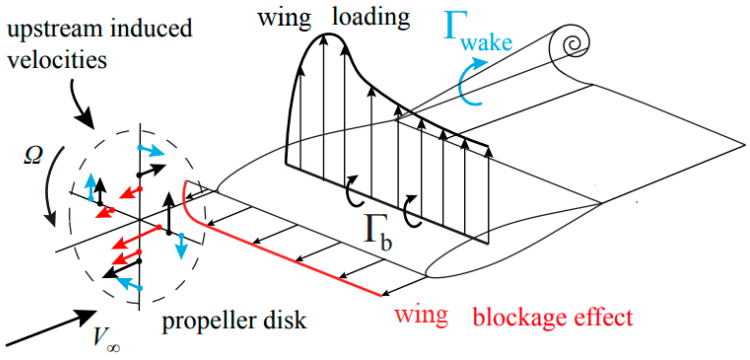

Figure 1. Propeller–wing interaction diagram [33].

2.2. Effects of the Propeller's Slipstream on the Wing

The propeller has a downstream impact on the wing by altering the inflow over it. The axial and swirl velocity created by the propeller have a distinct influence on the flow over the wing. The axial velocity has a significant impact on the local forces because it increases the dynamic pressure over the wing [10]. The swirl velocity changes the angle of attack in different parts of the wing. The upward blade raises the local wing angle of attack, while the downward blade reduces it [10]. When the wing is at a positive angle of attack, it produces positive lift, resulting in higher lift on the upward blade side and decreased lift on the downward blade side [10]. Figure 2 depicts the impact of the propeller slipstream on the wing.

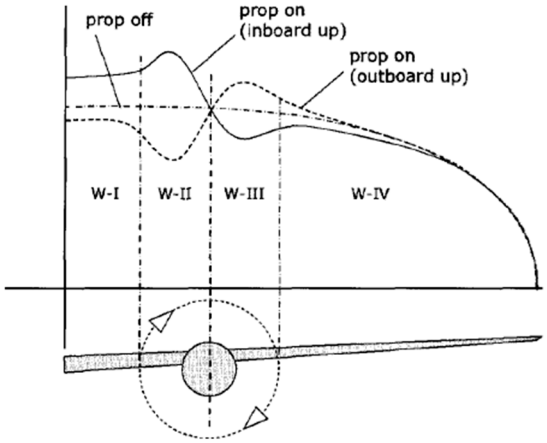

Figure 2. Lift distribution in wing sections influenced by propeller-slipstream-produced velocity [10].

The position of the propeller in relation to the wing is a factor that significantly influences the interaction. According to the findings indicated in the introduction, the stream-wise propeller position to the wing leading edge is set to a 1.0 radius of the propeller, and the vertical propeller position is set to a 0.6 radius of the propeller for high-lift propellers.

3. Methods

3.1. Frame for the Conceptual Design and Optimization of DEP Aircrafts

A wing with outstanding cruising performance is required for the design of DEP aircrafts [13]. Hence, the wing is initially created. Then, the DEP aircraft's wing area is reduced in comparison to the reference aircraft. Next, a CFD analysis of the performance of the small-wing aircraft in the cruise state is performed. If the performance of the new aircraft is inferior to that of the reference aircraft, a new wing design is created. The optimal design of the DEP in cruise is then carried out following the verification of the performance enhancement of the new aircraft. The DEP aircraft, designated as DEP_TP in

cruise, is equipped with two wing-tip propellers. Following the completion of the optimal design of DEP_TP, a CFD study of the DEP_TP is performed. DEP_TP will be the optimal configuration if its performance is superior to that of the reference aircraft throughout cruising, takeoff, and landing. The choice is based on the findings of [34], which show that pylons or nacelles reduce the lift–drag ratio in cruise. If DEP_TP cannot outperform the reference aircraft in overall cruising, takeoff, and landing performance, a further optimal design will be conducted with a high-lift propeller arrangement on the leading edge of the wing. The new configuration may be defined as DEP_HP. Following optimization, a further CFD analysis of DEP_HP will be carried out, and the performance of the DEP_HP will be obtained accordingly. The conclusion might be drawn by comparing the results to the performance of the reference aircraft. As a result, Figure 3 depicts the roadmap for the design of DEP aircraft.

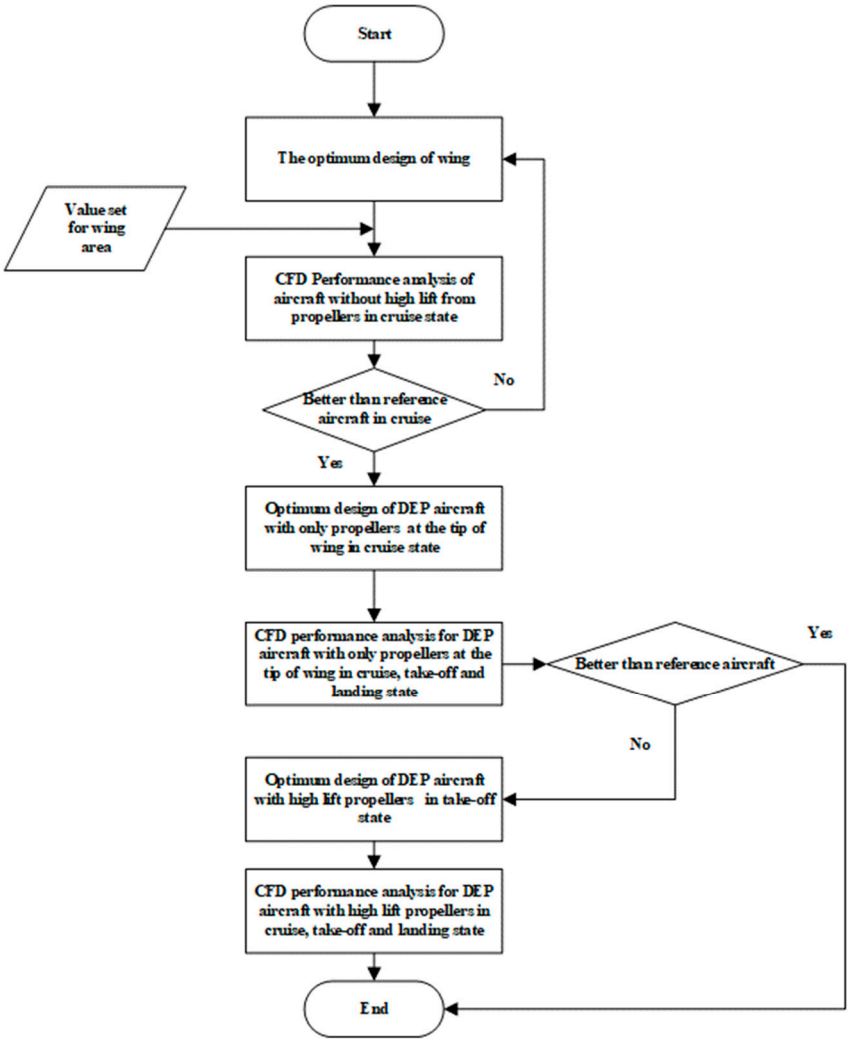

Figure 3. Roadmap for the design of DEP aircraft.

Figure 4 depicts the process of optimal design. Python Wrapper is used to conceptually create and optimize DEP settings. The method for balancing local and global search is DIRECT (Dividing Rectangles), which can be used easily as a global optimizer in Python programming [35]. After providing DIRECT with the design variables and the corresponding interval range, the optimizer will search as its strategy, and a candidate design scheme will be entered into the Python code. Using the script generated by this code, the wing or DEP aircraft will be represented in the OpenVSP as vortex lattices and propellers as actuator disks. Then, with VSPAERO called in script, the aerodynamic performance, such as lift coefficient, drag coefficient of wing or aircraft, and thrust coefficient, power coefficient, and

propeller efficiency, are obtained. In the case of constraints, the candidate design scheme is evaluated in code, and the workable plans are kept in a database. The optimum solution is established after the code quits.

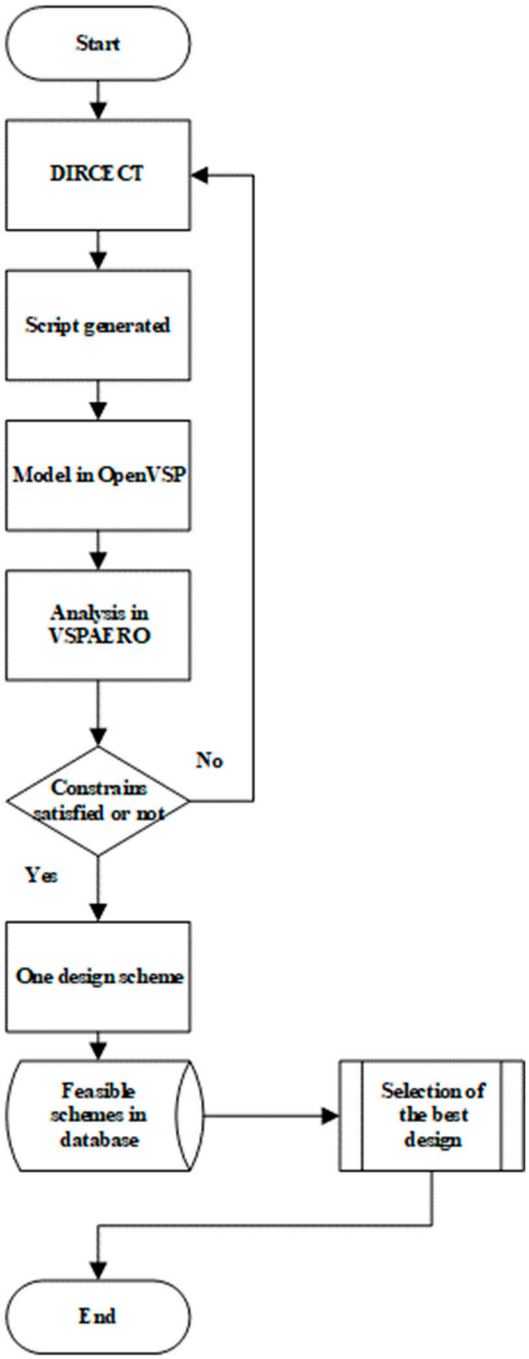

Figure 4. Process of optimum design.

Despite the low-order tool's neglect for the effect of viscosity, the aerodynamic performance of DEP aircrafts could be precisely predicted before stalling. The correctness of low-order tools in the interaction between the slipstream of propellers and the wing was already confirmed in [36,37] and other publications.

3.2. Validation of the Effectiveness of Low-Order and CFD Simulation for DEP Setup

As previously stated, OpenVSP and VSPAERO are the low-order analytic tools selected for this paper. The interaction between the slipstream of the propellers and the wing may

be quickly and reasonably precisely achieved in this tool by modeling DEP aircrafts in VLM and propellers in AD. The CFD tool here is STAR CCM+, which allows for an accurate examination of the aerodynamic performance of an aircraft. A propeller is represented as a virtual disk in STAR CCM+.

Here, simulations are performed to determine whether the tools mentioned above are efficient. Figure 5 depicts the simulation model, which comes from [10]. Moreover, the information from the wind tunnel test in [10] is also displayed in the tables below to evaluate the outcomes of the simulations.

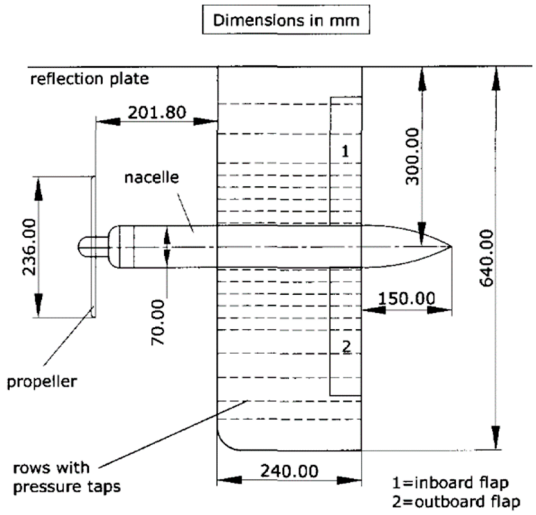

Figure 5. Model for calculation [10].

The simulation model in OpenVSP is displayed in Figure 6. The simulation's relevant inputs are V = 50 m/s, λ = 0.85, and RPS = 249 Hz. V stands for inflow velocity, λ for propeller advance ratio, RPS for propeller rotation speed, and BEM (blade element momentum) is used to calculate propeller thrust.

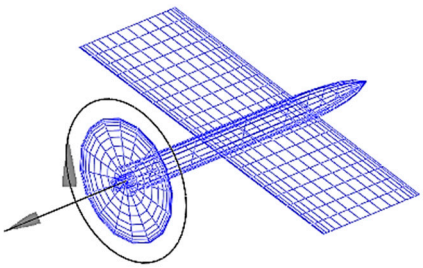

Figure 6. Model in OpenVSP.

Table 1 displays the outcomes from VSPAERO. It is obvious that the VSPAERO results are quite close to the data from the wind tunnel tests. The low-order tool could be utilized for the analysis of the interaction between a wing and a propeller's slipstream because the results are rather precise for such a small wing that is sensitive to factors.

Table 1. Results from VSPAERO.

α (°)	Method	C_L	C_D
0	Test	0.0055	−0.0986
	VSPAERO	−0.0028	−0.0998
4	Test	0.3135	−0.0916
	VSPAERO	0.3026	−0.0873

The virtual disk and k-ε turbulence model are used in STARCCM+ to create a steady simulation. Figure 7 depicts the model. More than 1.2 million cells make up the grid, and they are polyhedral cells. The model's border is configured as a smooth wall with no slide, and the y plus at the wall is configured as 100. Table 2 displays the results from the CFD simulation.

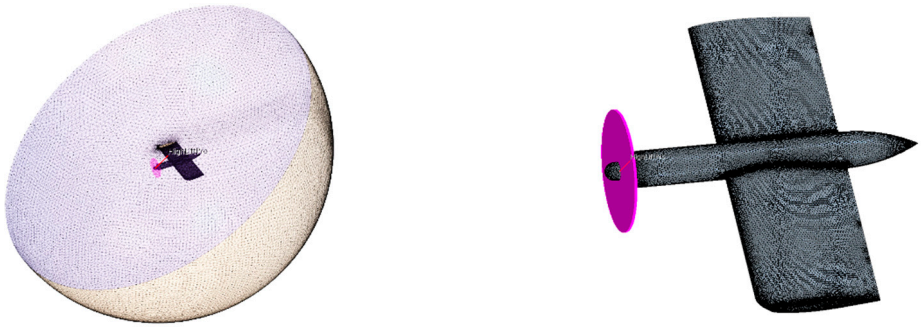

(**a**) (**b**)

Figure 7. Model in STAR CCM+: (**a**) Region model in STAR CCM+; (**b**) Model of wing and virtual disk of propeller in STAR CCM+.

Table 2. Results from CFD.

α (°)	Method	C_L	C_D
0	Test	0.0055	−0.0986
	CFD	−0.0070	−0.0948
4	Test	0.3135	−0.0916
	CFD	0.3096	−0.0862

For such a parameter-sensitive small wing, the CFD results have good agreement with the wind tunnel test; therefore, the steady simulation in CFD might be used for concept design scheme evaluation. It should be noted that the C_D in Tables 1 and 2 is the combined effect of propeller thrust and aerodynamics, hence its value may be negative.

4. Design and Optimization of DEP Aircraft

4.1. Reference Aircraft

The four-seat full electric general aircraft known as RX4E in the Liaoning General Aviation Academy served as the reference aircraft for the construction of a DEP fixed-wing aircraft. In Figure 8, the airplane is depicted. The DEP aircraft's fuselage shares the same dimensions as the RX4E fuselage to simplify the design. Moreover, the DEP aircraft shares an aerodynamic design with the X-57 (in Figure 9).

Figure 8. RX4E in LGAA.

Figure 9. X-57.

4.2. Conceptual Design and Optimization of DEP Aircraft

4.2.1. Design and Optimization of Wing

The wing is designed and optimized using the process depicted in Figure 4. The wing is defined by the following variables: wing root chord, wing tip chord, half of wing span, wing geometric twist angle, wing incidence angle, and wing dihedral angle. Table 3 shows the variable interval range. Except for the wing variables, the sweep angle in 1/4 chord of the wing is set to zero, and the airfoil of the wing is the same as RX4E. The objective of wing optimization is to maximize its lift–drag ratio at a 0° attack angle.

Table 3. Variables of wing.

Variables	Minimum	Maximum
Wing root chord (m)	1.20	1.50
Wing tip chord (m)	0.45	0.60
Half of wing span (m)	5.50	7.00
Wing geometric twist angle (°)	−3.00	0.00
Wing incidence angle (°)	0.00	3.00
Wing dihedral angle (°)	0.00	2.50

The optimal solution is selected from more than 4000 options once Python's optimum code terminates. Table 4 displays the optimal solution. The highest lift–drag value from the code is around 26.69.

Table 4. Optimal solution of wing.

Variables	Optimal Solution
Wing root chord (m)	1.21
Wing tip chord (m)	0.45
Half of wing span (m)	6.33

Table 4. *Cont.*

Variables	Optimal Solution
Wing geometric twist angle (°)	−1.75
Wing incidence angle (°)	2.60
Wing dihedral angle (°)	2.10

Naturally, as the wing area changes, so will the parameters, such as the root chord, tip chord, and wing span. However, the wing form is determined relative to the predetermined values of the wing aspect ratio, wing taper ratio, wing geometric twist angle, wing incidence angle, wing dihedral angle, and wing sweep angle in the 1/4 chord.

4.2.2. Aircraft with the Optimal Wing

The DEP aircraft will have a smaller wing area than the reference aircraft for the purpose of the DEP configuration study. Given the need for structural strength, the wing area ratio of the DEP design to the reference aircraft in this study was established at roughly 0.85. A simulation was ran in STAR CCM+ to evaluate the new aircraft's lift–drag performance. Figure 10 displays the new airplane in STAR CCM+.

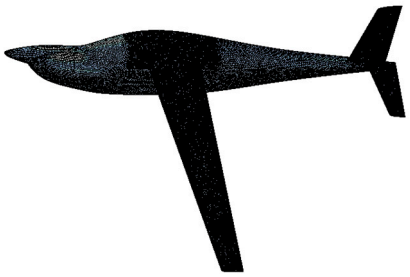

Figure 10. Surface grid of aircraft with the optimal wing.

The new aircraft's lift coefficient, drag coefficient, and lift–drag ratio in cruise condition is 0.4768, 0.0224, and 21.29, respectively. This new aircraft might serve as the basis for the DEP configuration since it has a lift–drag ratio that is 1.10 times that of the RX4E in cruise.

4.2.3. Design and Optimization of DEP_TP

The layout of the propellers on the wing is the subject of the DEP configuration design and optimization. The diameter and advance ratio of the propeller are chosen as variables for the optimal design of DEP_TP. Table 5 shows the design variable interval ranges. A three-blade propeller with a certain performance is chosen in order to lessen the impact of the propellers' performance. Figure 11 depicts its performance. According to the similarity theory for propellers, a propeller's performance is fundamentally fixed, and its performance is directly connected to its advance ratio in certain Re and Mach ranges. Yet, the propeller's size and working condition may be modified according to the demands of the design. Moreover, all propellers rotate inboard and up.

Table 5. Variables for DEP_TP.

Variables	Minimum	Maximum
Diameter of propeller (m)	0.70	1.50
Advance ratio of propeller	0.63	0.96

The highest lift–drag product with propeller efficiency at an attack angle of 0 degree is set as the optimal objective of DEP_TP in Formula (1). The optimal objective is a comprehensive result of aerodynamics and propulsion, and it is reasonable for evaluating the interaction between the slipstream of the propellers and the wing. In a sense, the optimum objective is an indicator of the DEP aircraft range because it is directly related to the power consumption of the DEP aircraft in cruise. The identical parameter used in this paper's optimum objective was used in the performance evaluation of a tractor propeller–wing system and a UAV in [13,38].

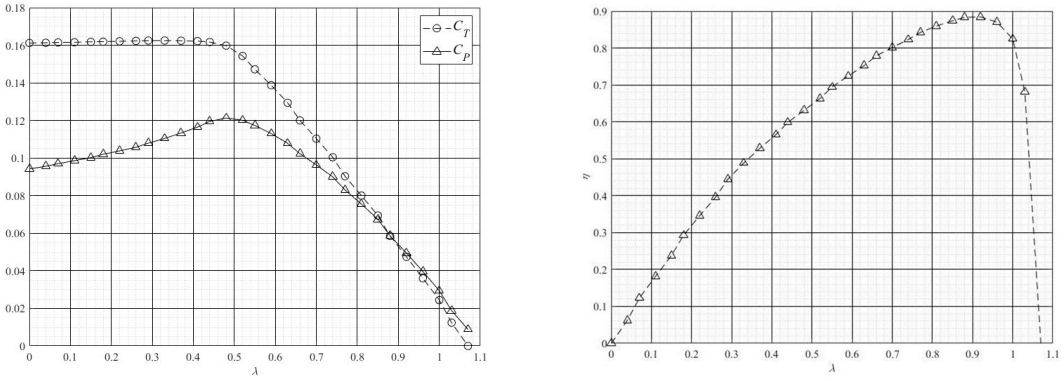

(**a**) (**b**)

Figure 11. Performance of propeller: (**a**) C_T and C_P with λ; (**b**) η with λ.

Force balance is the constraint condition during the optimum, and it is employed in Formulas (2) and (3) to calculate the propeller's advance ratio and cruising velocity. Without the restriction, the aerodynamic gain can be overestimated since the propeller's advance ratio directly affects the lift–drag ratio and the efficiency of the propeller.

The lift coefficient and drag coefficient of an aircraft should depend on the propellers' diameter and advance ratio, according to the discussion of the impact of propeller slipstream on wing in Section 2.2. The cruising speed of an aircraft might be obtained from Formula (2) in Formulas (4) and (5). Additionally, Formulas (6)–(10) clarifies the relationship between the characteristics of the propellers and the drag coefficient and wing area of the aircraft based on Formula (3). As a result, the optimal objective of the DEP aircraft in cruise in Formula (1) is to match the optimal propeller characteristics to the aircraft.

$$\eta_T = \eta \frac{C_L}{C_D} \tag{1}$$

$$\mathrm{L} = \mathrm{W} \tag{2}$$

$$\sum T = D \tag{3}$$

$$L = C_L \cdot \frac{1}{2} \rho V^2 S = W \tag{4}$$

$$\mathrm{V} = \sqrt{\frac{2 \cdot W}{C_L \rho S}} \tag{5}$$

$$\lambda = \frac{V}{n_s D_p} \tag{6}$$

$$C_D = \frac{D}{\frac{1}{2} \rho V^2 S} \tag{7}$$

$$C_T = \frac{T}{\rho {n_s}^2 {D_p}^4} \tag{8}$$

$$2 \cdot C_T \cdot \left(\rho {n_s}^2 {D_p}^4\right) = 2 \cdot C_T \cdot \rho \left(\frac{V}{\lambda}\right)^2 \cdot {D_p}^2 = C_D \cdot \frac{1}{2} \rho V^2 S \tag{9}$$

$$\frac{C_T}{\lambda^2} {D_p}^2 = \frac{C_D \cdot S}{4} \tag{10}$$

The optimal solution is obtained from more than 1700 solutions after the optimal code terminates. Table 6 shows the optimal solution. According to the analysis results in Python code, the lift–drag ratio advantage is around 1.05 times more than that of the aircraft in Figure 10, and the efficiency gain is roughly 1.19 times greater than that of the RX4E.

Table 6. Optimal solution of DEP_TP.

Variables	Optimal Solution
Diameter of propeller (m)	1.067
Advance of propeller	0.895

Additionally, a CFD simulation is ran, as shown in Figure 12. A motor nacelle is added to the new layout based on Figure 10. The cruise lift–drag ratio from CFD for a comparable arrangement in Figure 12 without propeller but with nacelle is 20.82 at a speed of around 62 m/s. The cruise lift–drag ratio from CFD is 21.66 at 61 m/s, with a propeller advance ratio of 0.90 for the setup shown in Figure 12. As a consequence, according to the CFD simulation, the lift–drag advantage for the configuration in Figure 12 is around 1.7% bigger than that for Figure 10, and the efficiency gain for Figure 12 is nearly 19% higher than that for RX4E. It should be mentioned that the aerodynamic advantage of the 1.017 times lift–drag ratio may be divided into two parts: 0.978 from the extra nacelle and 1.040 from the propeller's slip-stream.

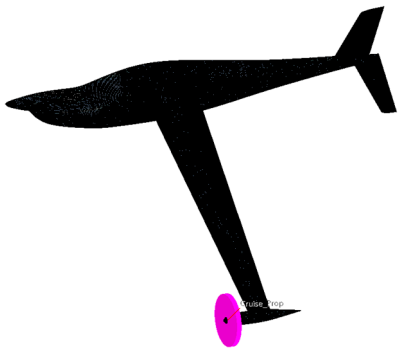

Figure 12. DEP_TP's model in STAR CCM+.

In addition to the performance in cruise, the performances in takeoff and landing are also obtained from two further CFD simulations. The takeoff speed is around 33.0 m/s with a flap deflection of 10° and an attack angle of 8°, which is somewhat less than the tail down angle. The landing speed is around 32.3 m/s, with a flap deflection of 25° and an attack angle of 8°. According to a CFD simulation, the RX4E's takeoff and landing velocities are 31.45 m/s and 29.52 m/s, respectively. In comparison to RX4E, DEP_TP's takeoff and landing speeds are a little higher. So, in a sense, the DEP_TP's ground run distance during takeoff and landing should be greater than that of RX4E. It is necessary to lay out high-lift propellers in order to improve DEP_TP's takeoff and landing performance.

4.2.4. Design and Optimization of DEP_HP

The optimum purpose of DEP_HP is to maximize the lift coefficient during takeoff and landing by minimizing the takeoff and landing velocity. The propellers used to create DEP_HP are the same as those used to design DEP_TP. The propeller diameter and advance ratio are further design variables. Table 7 specifies the interval ranges for the design variables. Section 2.2 specifies the streamwise and vertical positions of high-lift propellers. The axis of propeller rotation is parallel to the aircraft's longitudinal axis. All the propellers rotate inboard and up. The parameters are the same for every high-lift propeller. The state of flight is set at an attack angle of 8 ° but without a deflection of flaps. Hence, C_L may be accurately approximated without turbulence separation's influence.

Table 7. Variables for DEP_HP.

Variables	Minimum	Maximum
Diameter of high-lift propeller (m)	0.40	1.00
Advance of high-lift propeller	0.46	0.96
Advance of wing-tip propeller	0.46	0.96

The length of the span remaining after deducting the diameter of the wing-tip propeller and the fuselage width is one constraint. Another constraint is the Mach number of the blade tip, which is used to present noise restriction. The range of the advance ratio of the propeller is then calculated using the noise constraint.

The highest lift coefficient to diameter of high-lift propellers is depicted in Figure 13 based on the code. Figure 14 depicts the lift coefficient to advance ratio of high-lift propellers and wing-tip propellers in a setup with a high-lift propeller diameter of 0.967 m.

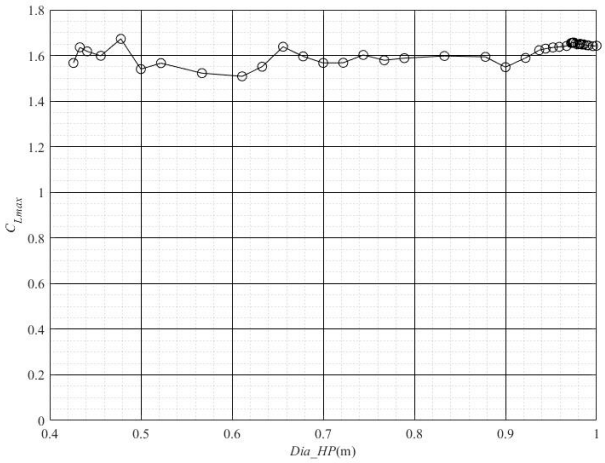

Figure 13. The maximum C_L with diameter of high-lift propeller.

From Figure 13, it can be concluded that the diameter of high-lift propellers has little effect on the maximal lift coefficient of DEP_HP. Nevertheless, it should be emphasized that the drag coefficient would invariably be underestimated since C_{D0} related to the pylons of high-lift propulsions will be reduced because their impact on the wing was disregarded in VSPAERO. With pylons on the wing, the lift–drag ratio will decrease significantly compared to [33]. Thus, as the number of pylons increases, the diameter of the high-lift propeller will have a significant impact on the DEP's cruise performance. Figure 15 depicts the results of two CFD simulations with various numbers of high-lift propellers. It reveals that the cruise lift–drag ratio is 10.7 for the 24 high-lift propellers configuration with a wing-tip propeller advance ratio of 0.85, and 17.08 for the 10 high-lift propeller configuration, with a wing-tip propeller advance ratio of 0.88.

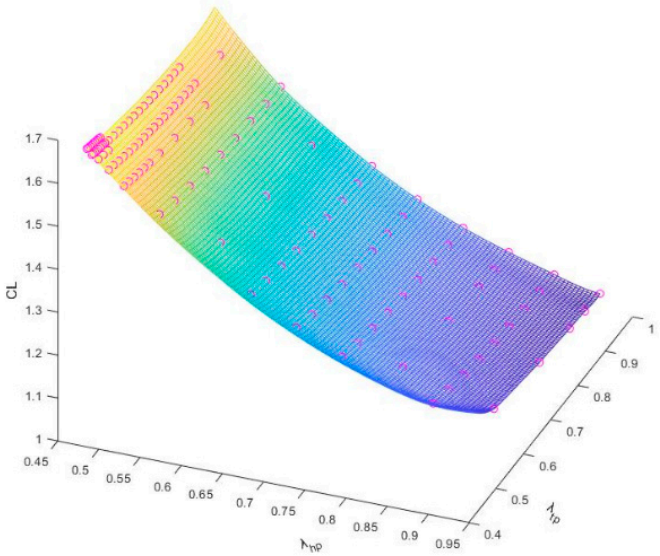

Figure 14. C_L with $\lambda_{\_tp}$ and $\lambda_{\_hp}$.

(**a**) (**b**)

Figure 15. Different configurations of DEP_HP: (**a**) Cruise configuration with 24 high-lift propellers pylons; (**b**) Cruise configuration with 10 high-lift propellers pylons.

The decrease in the advance ratio of high-lift propellers has a significant impact on the DEP aircraft's lift coefficient, according to Figure 14. This makes sense since, for a given inflow velocity, an increase in the spinning speed of a propeller's slipstream will result in a greater axis velocity.

Ultimately, a DEP HP configuration is obtained, as seen in Figure 16. On the leading edge of the wing, there are 10 high-lift propellers with a 0.944 m diameter.

Figure 16. DEP_HP's model in STAR CCM+.

Two further CFD simulations are conducted to evaluate the takeoff and landing performances of DEP_HP. Figure 17 depicts the rise in axial velocity caused by the propeller's action, and Figure 18 depicts the local change in the attack angle caused by the propeller's spin. The lift coefficient of DEP_HP in takeoff is 2.404, according to the CFD simulation with a high-lift propeller advance ratio of 0.5 and a wing-tip propeller advance ratio of 0.88. Moreover, the other CFD simulation with the identical propeller operating conditions yielded a lift coefficient of 2.838 for DEP_HP during landing. For takeoff and landing, the acceleration is 2.83 m/s^2 and 1.97 m/s^2, respectively. The speed of takeoff is approximately 27.6 m/s, while the speed of landing is around 25.4 m/s. As mentioned in Section 4.2.3, the RX4E's takeoff and landing velocities are 31.45 m/s and 29.52 m/s, respectively. Thus, DEP HP's takeoff and landing are superior to RX4E's.

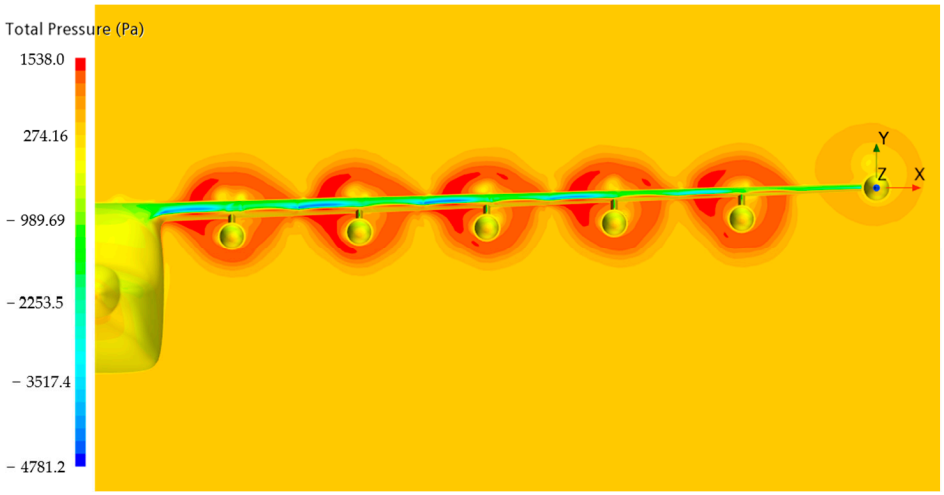

Figure 17. The rise in total pressure in the region of the propeller's activity in STAR CCM+.

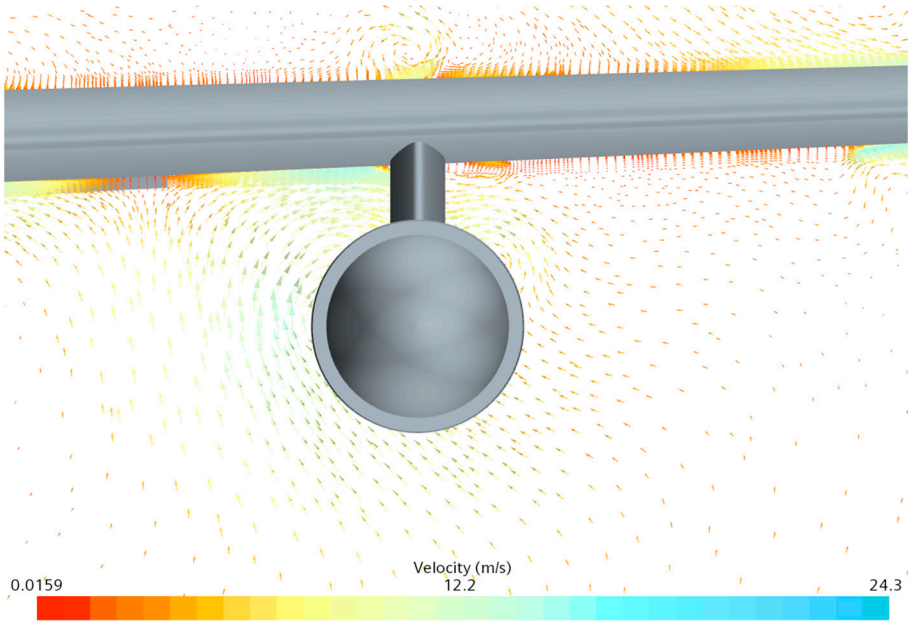

Figure 18. Change in angle of attack in the area of propeller motion in STAR CCM+.

Hence, it can be concluded that DEP_HP's η_T in cruise will be about 1.06 times that of RX4E without a degradation in the takeoff and landing performance compared to RX4E. The cruise performance gain in DEP_HP is achievable for 0.89 times the variance in aerodynamics and 1.19 times the benefit in propulsion efficiency.

5. Further Evaluation of DEP Aircraft

5.1. Investigation of Stall Characteristics for DEP Aircraft

The stall characteristic is another important performance indicator for airplanes. As a result, the stall characteristic of DEP aircrafts must be obtained. According to CCAR-23-R4, the stall speed of an aircraft must be achieved with the propulsion systems' power set at idle or zero thrust. The advance ratio of the propellers for the wing-tip propellers in DEP_TP and DEP_HP should be adjusted to 1.07 for zero thrust. The V_{S1}, in which flap deflection does not occur, is selected to assess the stall characteristics of various aircrafts since it is difficult to properly simulate the lift coefficient and drag coefficient for the takeoff and landing configuration with a large flap deflection. Furthermore, it should be noted that during the simulation of V_{S1}, all of the high-lift propellers in DEP_HP are folded up similar to how they are in the X-57's cruising state. Figure 19 depicts the C_L together with the attack angle for various aircrafts. According to Figure 19, the stall attack angle for the DEP aircraft is a little bit smaller than that of RX4E. Additional calculations show that the stall speeds of DEP_TP and DEP_HP are almost equal and are roughly 1.1 times those of RX4E.

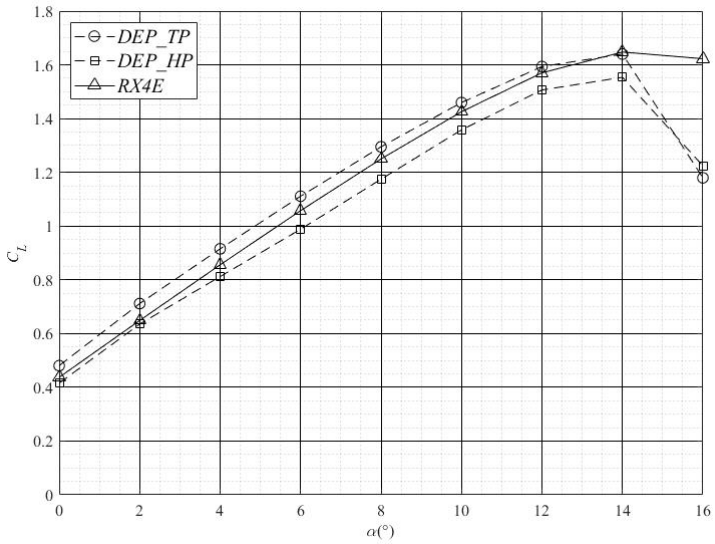

Figure 19. Stall characteristics of different aircrafts.

5.2. Assessment of the Power Needs for DEP Aircraft

The power requirements for the DEP_HP during takeoff and landing were also determined by the CFD simulation. At the takeoff condition, the power need is at its highest and is around twice that of RX4E. The weight of propulsion in DEP_HP will rise significantly for the same power–weight ratio. Nonetheless, DEP aircrafts would be viable if propulsion with a power–weight ratio greater than 2 kW/kg was used because the power–weight ratio of an electric motor today can range from 1 to 5 kW/kg [39], and the RX4E has a power–weight ratio of roughly 1 kW/kg. For the DEP aircraft, a high power–weight propulsion is essential.

6. Conclusions and Discussion

This paper provided a conceptual design and optimization approach for DEP aircrafts. Based on the CFD simulation of the optimal DEP aircraft, it was established that the cruise lift–drag ratio of the DEP aircraft could not be increased by adding high-lift propulsion system nacelles on the wing, but the efficiency of the DEP could be enhanced owing to the high-efficiency propeller and the strategy used in the optimal design process to capture the high-efficiency operating point of the propeller.

Based on the CFD simulation of the optimal DEP aircraft in cruise, takeoff and landing, the following conclusions were drawn:

- Under the restrictions of force balance, the increase in the cruise lift–drag ratio that results from the use of the wing-tip propellers that spin inboard and up is finite. It barely amounts to 1.7%, which is far less than the 5–10% discovered in the research of reference [8];
- Due to the use of high-lift propellers, the lift coefficient of the DEP aircraft during take-off and landing could be satisfactorily enhanced. However, compared to conventional airplanes, DEP aircrafts would use nearly twice as much power;
- A DEP aircraft with a small wing area will have a greater stall speed than a conventional aircraft. Because the stall speed could only be attained with the propulsion systems' power set to zero thrust or idle.

The method described in this study may be utilized to enhance the cruise performance of a DEP aircraft in contrast to an aircraft with a conventional configuration. There could be an electric aircraft type with reduced cruise power consumption in the general aviation industry soon. Nonetheless, there are a few issues that need be addressed in the subsequent study:

- When optimizing wings, the airfoil is ignored in favor of the wings' planar shape. This can make it more difficult to choose the superior wing with outstanding cruising performance;
- Due to the low speed of a general aviation aircraft and the little variations in propeller size, the effects of the Reynolds number and Mach number on the performance of the propeller are disregarded in this study. The propeller performance could be overstated;
- The energy loss due to propeller thrust variability with time is neglected in the steady CFD simulation. Hence, the lift–drag ratio and propeller efficiency may be exaggerated;
- The lift–drag ratio of DEP aircrafts is sensitive to the size of the motor, and the lift–drag ratio of the DEP aircraft here is based on the popular motor size of 9-12 inches. Hence, for the alternative DEP arrangement with various size motors, the lift–drag ratio may be somewhat altered.

Author Contributions: J.W. presented the concepts, created the methodology, created the software, carried out validation, put together the models, did formal analysis, carried out the study, and completed data curation. F.G. took part in the methodology's creation. S.L. conducted the inquiry and assisted with the validation. F.Y. specified the conception, gave permission for the formal analysis, assisted with the investigation, and supplied the research's resources. The first draft of the text was prepared with input from all writers. The paper was reviewed and edited by J.W. and F.Y. F.Y. performed the supervision and supplied the financing acquisition for the project, and all writers took part in its visualization. The management of the project was done by J.W. and F.Y. All authors have read and agreed to the published version of the manuscript.

Funding: This research received no external funding.

Institutional Review Board Statement: Not applicable.

Informed Consent Statement: Not applicable.

Data Availability Statement: All data used during the study appear in the submitted article.

Conflicts of Interest: The authors declare no conflict of interest.

References

1. Huang, J.; Yang, F.T. Development and challenges of electric aircraft with new energies. *Chin. J. Aeronaut.* **2016**, *37*, 57–68.
2. Benjamin, J.B.; Joaquim, R.R.A.M. Electric, hybrid, and turboelectric fixed-wing aircraft: A review of concepts, models, and design approaches. *Prog. Aerosp. Sci.* **2019**, *104*, 1–19.
3. Nicholas, K.B.; Craig, L.N.; Frank, P.J.; Yasky, R.; Woodham, K.; Fell, J.; Litherland, B.; Loyselle, P.; Provenza, A.; Kohlman, L.; et al. Overcoming the adoption barrier to electric flight. In Proceedings of the 54th AIAA SciTech Forum Aerospace Sciences Meeting, San Diego, CA, USA, 4–8 January 2016.
4. Wang, K.; Zhou, Z.; Fan, Z.; Guo, J. Aerodynamic design of tractor propeller for high-performance distributed electric propulsion aircraft. *Chin. J. Aeronaut.* **2021**, *34*, 20–35. [CrossRef]

5. Huang, J. Survey on design technology of distributed electric propulsion aircraft. *Chin. J. Aeronaut.* **2021**, *42*, 13–29.
6. Kim, H.D.; Perry, A.T.; Ansell, P.J. A Review of Distributed Electric Propulsion Concepts for Air Vehicle Technology. In Proceedings of the 2018 AIAA/IEEE Electric Aircraft Technologies Symposium, Cincinnati, OH, USA, 9–11 July 2018.
7. Deere, K.; Viken, J.; Viken, S.; Carter, M.B.; Wiese, M.; Farr, N. Computational Analysis of a Wing Designed for the X-57 Distributed Electric Propulsion Aircraft. In Proceedings of the 35th AIAA Applied Aerodynamics Conference AIAA AVIATION Forum, Denver, CO, USA, 5–9 June 2017.
8. Borner, N.K.; Patterson, M.D.; Viken, J.K.; Moore, M.D.; Bevirt, J.; Stoll, A.M.; Gibson, A.R. Design and Performance of the NASA SCEPTOR Distributed Electric Propulsion Flight Demonstrator. In Proceedings of the 16th AIAA Aviation Technology, Integration, and Operations Conference, Washington, DC, USA, 13–17 June 2016.
9. Deere, K.; Viken, S.; Carter, M.; Viken, J.K.; Cox, D.E.; Wiese, M.R.; Farr, N.L. Computational Component Build-up for the X-57 Maxwell Distributed Electric Propulsion Aircraft. In Proceedings of the 2018 AIAA Aerospace Sciences Meeting, Kissimmee, FL, USA, 8–12 January 2018.
10. Veldhuis, L.L. Propeller Wing Aerodynamic Interference. Doctoral Thesis, Faculty of Aerospace Engineering, Delft University of Technology, Delft, The Netherlands, 2005.
11. Sinnige, T.; van Arnhem, N.; Stokkermans, T.C.A.; Eitelberg, G.; Veldhuis, L.L.M. Wingtip-Mounted Propellers: Aerodynamic Analysis of Interaction Effects and Comparison with Conventional Layout. *J. Aircr.* **2019**, *56*, 295–312. [CrossRef]
12. Stokkermans, T.C.; Arnhem, N.V.; Sinnige, T.; Veldhuis, L.L. Validation and Comparison of RANS Propeller Modeling Methods for Tip-Mounted Applications. *AIAA J.* **2018**, *57*, 1–15.
13. Willemsen, R. A Sensitivity Study on the Aerodynamic Performance of a Wingtip-Mounted Tractor Propeller-Wing System. Master's Thesis, Faculty of Aerospace Engineering, Delft University of Technology, Delft, The Netherlands, 2020.
14. Stoll, A.M. Comparison of CFD and Experimental Results of the LEAPTech Distributed Electric Propulsion Blown Wing. In Proceedings of the 15th AIAA Aviation Technology, Integration, and Operations Conference, Dallas, TX, USA, 22–26 June 2015.
15. Patterson, M.D.; Derlaga, G.M.; Borer, N.K. High-Lift Propeller System Configuration Selection for NASA's SCEPTOR Distributed Electric Propulsion Flight Demonstrator. In Proceedings of the 16th AIAA Aviation Technology, Integration, and Operations Conference, Washington, DC, USA, 13–17 June 2016.
16. Borner, N.K.; MOORE, M.D. Integrated Propeller-Wing Design Exploration for Distributed Propulsion Concepts. In Proceedings of the 53rd AIAA Aerospace Sciences Meeting, Kissimmee, FL, USA, 5–9 January 2015.
17. Patterson, M.D.; Borer, N.K.; German, B. A Simple Method for High-Lift Propeller Conceptual Design. In Proceedings of the 54th AIAA Aerospace Sciences Meeting, San Diego, CA, USA, 4–8 January 2016.
18. Rao, C.; Zhang, T.J.; Wei, C.H. Influence mechanism of propeller slipstream on wing of a distributed electric aircraft scheme. *Chin. J. Aeronaut.* **2021**, *42*, 157–167.
19. Shi, J.; Zhou, J.; Wu, L.N. Aerodynamic Investigation of a General Aviation Aircraft with Distributed Electric Propulsion. In Proceedings of the 2021 IEEE International Conference on Advances in Electrical Engineering and Computer Applications (AEECA), Dalian, China, 27–28 August 2021.
20. Zhang, X.Y.; Gao, Z.H.; Lei, T.; Min, Z.; Lei, W.; Zhang, X. Ground test on aerodynamic-propulsion coupling characteristics of distributed electric propulsion aircraft. *Chin. J. Aeronaut.* **2022**, *43*, 406–416.
21. Cheng, Z.Y.; Yang, Y.X.; Zhang, X.C.; Yu, L.F.; Ye, B. Rapid evaluation and method for aerodynamic characteristics of distributed electric propulsion aircraft concept scheme. *J. Beijing Univ. Aeronaut. Astronaut.* **2021**, *OL*, 1–16.
22. Yang, W.; Fan, Z.L.; Wu, W.H.; Lei, Y.U. Optimal design of distributed propeller layout considering slipstream effect. *Acta Aerodyn. Sin.* **2021**, *39*, 71–79.
23. Pela, P.; Leise, P.; Meck, M. Sustainable aircraft design—A review on optimization methods for electric propulsion with derived optimal number of propulsors. *Prog. Aerosp. Sci.* **2021**, *123*, 10074.
24. Erhard, R.M.; Clarke, M.A.; Alonso, J.J. A Low-Cost Aero-Propulsive Analysis of Distributed Electric Propulsion Aircraft. In Proceedings of the AIAA Scitech 2021 Forum, Virtual Event, 11–15 & 19–21 January 2021.
25. Lei, Y.; Yang, W.Q.; Huang, Y.Y. Aerodynamic performance of distributed electric propulsion with wing interaction. *J. Zhejiang Univ. Sci. A* **2022**, *23*, 27–39. [CrossRef]
26. Olichevis Halila, G.L.; Neves Pedreiro, L.; Silveira Molina, E.; Savio, M.C. Efficient Aerodynamic Analysis for Propeller Aircraft Including Viscous Effects. In Proceedings of the AIAA SCITECH 2022 Forum, Virtual, San Diego, CA, USA, 3–7 January 2022.
27. D'angelo, B.K. Low-Order Modeling of Propeller-Wing Interaction Using a Modified Weissinger Method. Master's Thesis, North Carolina State University Aerospace Engineering, Raleigh, NC, USA, 2021.
28. Alba, C.; Elham, A.; German, B.; Veldhuis, L.L. A Surrogate-Based Multi-Disciplinary Design Optimization Framework Exploiting Wing-Propeller Interaction. In Proceedings of the 18th AIAA/ ISSMO Multidisciplinary Analysis and Optimization Conference, Denver, CO, USA, 5–9 June 2017.
29. Xue, C.; Zhou, Z.; Fan, Z.Y.; Li, X. Design of target propeller slipstream under propeller-wing interaction. *J. Aerosp. Power* **2021**, *36*, 104–118.
30. Alvarez, E.J.; Ning, A. Development of a Vortex Particle Code for the Modeling of Wake Interaction in Distributed Propulsion. In Proceedings of the 2018 Applied Aerodynamics Conference, Atlanta, GA, USA, 25–29 June 2018.
31. Alvarez, E.J.; Ning, A. Modeling Multirotor Aerodynamic Interactions through the Vortex Particle Method. In Proceedings of the AIAA Aviation 2019 Forum, Dallas, TX, USA, 17–21 June 2019.

32. Alvarez, E.J.; Ning, A. High-fidelity Modeling of Multirotor Aerodynamic Interactions for Aircraft Design. *AIAA J.* **2020**, *58*, 4385–4400. [CrossRef]
33. Arnhem, N.V.; Sinnige, T.; Stokkermans, T.C.; Eitelberg, G.; Veldhuis, L.L. Aerodynamic Interaction Effects of Tip-Mounted Propellers Installed on the Horizontal Tailplane. In Proceedings of the 2018 AIAA Aerospace Sciences Meeting, Kissimmee, FL, USA, 8–12 January 2018.
34. Wu, J.; Tong, S.X.; Gao, F.; Yin, C.; Yang, F.T. Comparison of Aerodynamic Layout Schemes of a Fuel Cell Aircraft. *Sci. Technol. Eng.* **2021**, *21*, 13574–13579.
35. Gablonsky, J.M.; Kelley, C.T. A Locally-Biased form of the DIRECT Algorithm. *J. Glob. Optim.* **2001**, *21*, 27–37. [CrossRef]
36. Bohari, B.; Bronz, M.; Benard, E.; Borlon, Q. Conceptual Design of Distributed Propeller Aircraft: Linear Aerodynamic Model Verification of Propeller-Wing Interaction. In Proceedings of the 7th European Conference for Aeronautics and Aerospace Sciences (EUCASS), Milan, Italy, 3–6 July 2017.
37. Stone, R.H. Aerodynamic Modeling of the Wing-Propeller Interaction for a Tail-Sitter Unmanned Air Vehicle. *J. Aircraft.* **2008**, *45*, 198–210. [CrossRef]
38. Ma, Y.; Zhang, W.; Zhang, Y.; Zhang, X.; Zhong, Y. Sizing Method and Sensitivity Analysis for Distributed Electric Propulsion Aircraft. *J. Aircr.* **2020**, *57*, 730–741. [CrossRef]
39. Bright, A.A.; Clara, G. Electric aviation: A review of concepts and enabling technologies. *Transp. Eng.* **2022**, *9*, 100134.